Probing Colloidal Assembly on Non-Axisymmetric Droplet Surfaces via Electrospray

*Joseph M. Prisaznuk, Peter Huang, Xin Yong[+], and Paul R. Chiarot**

Department of Mechanical Engineering, State University of New York at Binghamton, 4400 Vestal Parkway East, Binghamton, New York 13902, United States

Abstract

Microparticles trapped on the surface of a sessile droplet interact via electrostatic and capillary forces. The assembly of colloids at a fluid-fluid interface is governed by particle size, surface chemistry, and contact line roughness. We created non-spherical droplets using surface energy patterning and delivered microparticles to the liquid-air interface with electrospray atomization. Using a water droplet as the target, the particle assembly was observed over time. We found that the underlying surface energy pattern significantly influenced the colloidal assembly and drove particles toward the center of the droplet. The particles were arranged into a single, non-close-packed cluster with local hexagonal ordering, but left a clear region with very few particles near the contact line. This depletion region is attributed to long-range electrostatic repulsion from the photoresist used to create the surface energy pattern, which retained electric charge from the electrospray. To understand the effect of electrostatic interactions, we explored target droplets with dissimilar dielectric properties. Using patterned substrates and electrospray for particle deposition, we can harness the assembly of colloids at a fluid interface to build repeatable monolayer patterns.

Keywords

electrospray, interface, self-assembly, colloid, sessile droplet, evaporation

Main Text

Introduction

Interactions between micro- and nano-scale particles at a fluid-fluid interface have been studied for over four decades.[1] Typically, the interface is formed between an aqueous (polar) phase and a non-polar phase, such as air or oil. Colloidal particles reduce the total interfacial energy of the system when straddling the interface and thus become effectively trapped at the interface. For micrometer-sized particles, this trapping energy is several orders of magnitude higher than thermal energy $\sim k_{\mathrm{B}}T$, rendering the adsorption irreversible. The ensuing dynamics at the interface have been thoroughly investigated for particles of various compositions, shapes, and sizes.[2–4] Non-uniform wetting of spherical particles due to surface roughness can lead to the formation of linear aggregates via anisotropic capillary interactions.[5] The mechanism preventing clustering of these structures is attributed to electrostatic dipole-dipole repulsions between particles,[6] leading to a stable potential energy minimum. The precise location of electric charges on interface-bound colloids remains elusive,[7–10] but it is widely accepted that electric charges lead to isotropic repulsion, keeping the particles separated. On curved interfaces with anisotropic curvature, the orientation of capillary forces can be strictly controlled.[11,12] This was shown experimentally by Ershov *et al.*[13] through the formation of cubic arrangements of spherical particles, in which interaction strength between particles was found to be directly proportional to the deviatoric curvature of the liquid interface. Furthermore, their experiments demonstrated the transition from cubic lattice ordering to hexagonal ordering when interfacial particle density increases, as isotropic short-range repulsions dominate under confinement.

The internal flow and final deposition pattern of an evaporating sessile droplet containing solid particles can vary significantly based on the droplet composition (aqueous vs. organic),

environmental conditions, and surfactant concentration.[14] Particle-laden droplets with a pinned contact line produce a “coffee-ring” deposit, caused by an outward convective flow generated in response to a higher evaporation rate at the contact line.[15] Temperature variation between the contact line and droplet apex would cause a strong thermal Marangoni flow to develop in millimeter-scale droplets. However, this flow may be suppressed by trace amounts of surfactants.[16] Experiments with surfactants introduced in the bulk have shown that the surfactant’s molecular composition is crucial. Large, non-ionic surfactants render the interface rigid and tend to reduce the bulk and interfacial flow.[17] Conversely, anionic surfactants such as SDS can continuously desorb into the droplet bulk and adsorb at the contact line throughout evaporation, leading to a sustainable surface tension gradient with a corresponding Marangoni flow towards the droplet apex. Similar behavior has been observed on droplets where the surfactant is introduced directly to the interface via electrospray;[18] the interfacial flow is suppressed by non-ionic Tween 80 and enhanced by SDS. In the pursuit of building well-ordered particle monolayers through the evaporation of colloidal droplets, the complex influences of the bulk flow can be avoided by taking advantage of a system with particles located only at the droplet interface.[19]

Interfacial self-assembly of colloidal particles has been used to fabricate complex optical devices and coatings.[20–22] In particular, two-dimensional colloidal crystals are significant for their unique optical properties; ordered arrays of nanoparticles diffract light differently based on the particle size and spacing. The structural color of 2D colloidal crystals can be visually detected and may be used for chemical sensing applications.[23–25] Colloidal crystals have also been used as an intermediate template for the synthesis of biological sensors.[26] Recently, monolayer colloidal crystals were similarly used as a template for building a UV sensitive

photonic device.[27] Close-packed metal nanoparticle monolayers also support localized surface plasmon resonance for plasmonic applications. Understanding the fundamental dynamics of interfacial colloidal assembly is crucial for the fabrication of these 2D devices. Our results may also have significance beyond this fundamental investigation, as our electrospray deposition process has the potential to be scaled up and refined for manufacturing.

Here, we use electrospray printing and geometrically controlled liquid-air interfaces to create self-assembled particle monolayers. Electrospray has the advantage of being a relatively non-intrusive method for depositing particles, without creating interactions between the target droplet and a secondary solvent. Additionally, it has the unique feature of imparting electric charge on the sprayed material and receiving substrate. With this novel technique to deliver particles on sessile droplets from the vapor phase, we are able to probe the interaction of polystyrene microspheres at aqueous and organic liquid-vapor interfaces. Furthermore, by using a circular pattern for spherical symmetry, and triangular and dumbbell patterns to create complex interfacial shapes, we investigate the long-ranged interactions between the patterned substrate and interfacial particles. While there have been studies[28,29] investigating interactions between the substrate and bulk particles on colloidal assembly, to our best knowledge the influence of the substrate's electrical properties on interfacial particle assembly has not been experimentally investigated. Through our experiments, we examine and identify how substrate repulsion influences monolayer assembly, resulting from the unique electrical properties of particles deposited by electrospray.

Experimental

Substrate Preparation

Glass substrates (25 mm x 75 mm x 2 mm) with a fluorine doped tin oxide (FTO) coating were purchased from MSE Supplies. Each substrate was cleaned via sonication in acetone and isopropyl alcohol, and fully dried using compressed nitrogen. Surface energy patterning was done by standard photolithography (Figure S1). Namely, negative photoresist (SU-8 2050) was spin-coated onto the substrate (500 rpm for 10 s, then 3000 rpm for 30 s) and then baked at 95 °C for 7 min (65 °C for 1 minute before and after to ramp up/down). The droplet contact line patterns were created by exposing the soft-baked substrate for 8 seconds to UV light (Suss Microtec MJB4 contact aligner). After a post-exposure bake at 95 °C for 6 min (again ramping up/down), the substrate was submerged in the first SU-8 developer dish for 6 min, then the second dish for one more minute. Finally, the substrate was rinsed with isopropyl alcohol, dried under a nitrogen flow, and hard baked for 15 min at 150 °C.

Deposition of Geometrically Controlled Target Droplet

The DI water used for target droplets had a resistance of 18 MΩ·cm. Trimethylolpropane ethoxylate triacrylate (ETPTA) was purchased from Sigma-Aldrich. Droplets of both liquids were placed onto the exposed FTO substrate patterns using a micropipette. The liquid was placed into the exposed regions incrementally, allowing time for the pattern to be fully covered. The droplet occasionally overfilled the pattern, which was fixed by pulling up some liquid through the pipette, forcing the droplet to recede. Therefore, the contact line was fixed at the top SU-8 edge for all experiments. The total deposited volume ranged from 1.5 to 2.5 µl for water, and 0.25 to 0.75 µl for ETPTA. For water experiments, the droplet side profile was continuously monitored with a CCD camera (QImaging); the height was measured and used to calculate the

instantaneous droplet volume over evaporation. The various droplet shapes were calculated numerically using a finite element method (Surface Evolver) to correlate height to volume.

Particle Suspension Preparation

Fluorescent polystyrene microparticles (2 μm diameter, 1 v/v % in water) were purchased from Thermo Fisher Scientific. The particles were internally dyed with a green fluorophore, with excitation/emission peaks of 468/508 nm. An unknown surfactant was included in the aqueous particle suspension. To prevent undesirable particle transport during experiments, the surfactant was removed by centrifugation and redispersion in DI water. The particles were diluted with DI water in a centrifuge tube to approximately 0.2 v/v % in water. Four centrifugation runs were completed for up to 30 min at 5510 RCF (Eppendorf Centrifuge 5418). The DI water was carefully removed at the end of each run, and the remaining particle pellet was resuspended in clean DI water. After the final run of removing the DI water, the particles were diluted in methanol. Sonication was used to remove aggregates that may have formed during centrifugation.

Electrospray Setup

The electrospray setup was similar to our previous experiments.[18] In this study, the suspension was sprayed while observing the target droplet *in situ* on an inverted microscope (Leica). The suspension was carried to a three-port manifold via polytetrafluoroethylene (PTFE) tubing, with the flow rate controlled by a syringe pump (Chemyx). The high voltage supply (Spellman 230-20R) was controlled with a basic DAQ (LabJack U3-HV) and connected to another manifold port. The final manifold port held a glass emitter with an inner diameter of 115 μm. The electrospray was formed at the tip of the emitter and exhibited a stable Taylor cone at approximately 2.3 kV and flow rates ranging between 0.5 – 2.0 μl/min. The Taylor cone was

monitored with a CMOS camera (Basler). The particles were primarily imaged with an electron-multiplying CCD camera (Andor).

Results and Discussion

Electrospray Targeting of Non-Axisymmetric Water Droplets

A schematic of our experimental setup is shown in **Figure 1**. The substrate is modified with a negative photoresist pattern to control the shape of a sessile droplet by pinning the contact line. Particles from the electrospray are initially encapsulated in the suspension solvent, which evaporates in flight. We use fluorescent polystyrene microparticles with a radius $a = 1$ μm in all experiments. Owing to their size, any deformation of the interface caused by gravitational body forces on the particles is negligible. The adsorption of particles at the interface is observed *in situ*, allowing us to infer the instantaneous particle density and decide when to stop the electrospray (Video S1). Particles are strongly restrained to the interface and rarely enter the bulk fluid. Additionally, the sample is shielded from ambient air flows on all four sides to prevent perturbations caused by air convection and non-uniform evaporation. An inverted fluorescence optical microscope is used to image the particles in conjunction with a side-view camera for monitoring the droplet volume evolution.

The initial droplet height is at least an order of magnitude larger than the maximum depth of field in our imaging system. Thus, it is not feasible for us to optically track the three-dimensional positions of all particles while the fluid interface evolves. Instead, we focus on quantifying the two-dimensional particle transport on the curved fluid interface over multiple length scales by utilizing two magnifications and analyzing regions that exhibit consistent behaviors over multiple experiments.

The dielectric properties of the substrate and target droplet strongly influence the spatial distribution of particles during deposition. The substrate is composed of three materials from bottom to top: a borosilicate glass base, an electrically conductive FTO (fluorine doped tin oxide) film, and a patterned photoresist (SU-8). The conductive FTO film is connected to a grounded aluminum base plate using copper tape. Under the influence of a strong electric field, the highly charged particles are directed to grounded surfaces.[30,31] The SU-8 photoresist acts as a surface energy pattern to modulate the wetting properties of the substrate, which defines the contact line (and consequently, the interface geometry) of the target droplet. Additionally, SU-8 is a cross-linked polymer and an excellent electrical insulator. During the initial spraying (within 1 sec), the accumulation of charges on the SU-8 changes the electric field near the substrate and begins to repel incoming particles. Subsequently, particles are preferentially deposited onto the droplet interface. This focusing effect intensifies over time, as electrostatic charges on the negative photoresist accumulate and push away incoming particles.

Figure 2 shows images of particles at a water-air interface. **Figure 2a** is a droplet with spherical cap symmetry, and **Figure 2b, c** have a triangular and a dumbbell-shaped footprint, respectively. A common phenomenon for all three shapes is the formation of a depletion region close to the contact line where very few particles reside. The depletion region is formed rapidly after stopping the electrospray, typically within 15-30 seconds (Video S2). The two-dimensional projected spacing between the contact line and particle assembly on the triangular and dumbbell droplets varies in space. Even accounting for the differences in *z*-height (small for the volumes shown), this spacing still varies along the contact line. The explanation for this effect may lie in the 2D pattern geometry and is not necessarily correlated to the local contact angle. In particular, particles are closer to concave regions of the contact line, and farther from convex regions.

The origin of the depletion region is likely the result of long-range repulsive electrostatic interactions. Positively charged ions accumulate on the insulating SU-8 photoresist, even after short spray times.[32,33] The rate of charge dissipation through the SU-8 to the grounded FTO film is much slower[34,35] than the droplet evaporation time scale, which ranged from 8 minutes for a 0.6 µl triangular droplet with RH = 10%, up to 26 minutes for a 2 µl spherical cap droplet with RH = 50%. In fact, based on the material properties for SU-8, we expect the surface charge to quickly saturate and maintain a relatively constant value over the course of evaporation. The electrical relaxation time of SU-8 can be estimated as the product of resistivity $\rho = 2.8 \times 10^{16}\ \Omega \cdot \mathrm{cm}$ and absolute permittivity $\epsilon = 4.1 \cdot \epsilon_0\ \mathrm{F/m}$, which is about 3 hours. Therefore, the charge delivered by the electrospray can be treated as quasi-static.

The charges deposited by the electrospray effectively form a parallel plate capacitor with the SU-8 as the dielectric material. The resulting static electric field drives the interfacial particles away from the contact line in all directions, confining them into a single assembly at the center of the interface. Therefore, the interfacial particle assembly and width of the depletion region are governed by the electrical properties of the substrate. If less charge is delivered to the substrate, or the delivered charge can be dissipated quickly, we expect the depletion region to be smaller as the static electric field would be weaker. This is observed on substrates without SU-8 as discussed in the following section.

Figure 3 shows the distribution of particles on the 3D droplet geometry at multiple stages of evaporation. As noted above, we numerically calculate the expected droplet interface shape using Surface Evolver. We apply a fixed boundary condition for the droplet contact line, matching our photoresist pattern geometry. Then, by introducing a volume constraint, the mesh converges to a minimum energy state after multiple iterations and refinement steps. This procedure is repeated

over the full range of volumes observed experimentally, at 0.01 µl increments. To produce the color map shown in **Figure 3**, we align images from the experiments with the mesh projected in 2D. The mesh elements are colored by the average intensity of the 8-bit image in each projected element. Finally, we adjust the calculated intensity for each element based on the ratio of the 2D mesh element area to the 3D area, to represent the expected particle density in 3D more accurately.

Considering different volumes for each shape, with the maximum range being 0.95 to 0.1 µl for the dumbbell, we see that the size of the depletion region does not change significantly during the majority of evaporation. This implies that the influence of evaporation on the interfacial particle assembly is minimal until the very late stage, where the contact line depins and the droplet detaches from the photoresist. At this point, a chaotic flow ensues and disturbs the particle assembly. To preserve the ordered structure, a thinner photoresist is ideal to allow for nearly complete evaporation without detachment of the contact line.

Consideration of Undesirable Marangoni Flows

Evaporating water droplets have been extensively studied and modeled.[15–17,36–38] In the absence of surfactants, a water droplet at the length scale used in our experiments should experience a strong, thermally induced Marangoni flow, which can drive particles to the droplet apex depending on the thermal conductivity of the substrate and fluid.[39] However, surfactant contamination of the target droplet is inevitable for our experiments conducted in ambient conditions. Any trace surfactants or oils from the pipette, substrate, or electrospray would greatly suppress the surface tension gradient due to temperature variation.[38] Without a method to accurately determine the concentration of trace surfactants in the target droplet, we devised four experiments to show that the central assembly is not attributed to Marangoni flows. As shown in

Figure 4, DI water droplets were sprayed at two different particle densities, with two substrates for each case. A bare FTO substrate (**Figure 4b, d**) was used to create spherical-cap sessile droplets with similar dimensions to the SU-8 patterned droplets (**Figure 4a, c**). The FTO substrate was cleaned via sonication in DI water and isopropyl alcohol. This procedure yielded a near 0° receding contact angle, so the contact line was fixed for the majority of evaporation. We observed no depletion region for the pattern-free droplets at two different particle densities, as charges arriving at the surrounding substrate can dissipate immediately. This implies that the particle assembly is dependent on the substrate properties rather than on an induced Marangoni flow and provides further evidence that the photoresist pattern has a significant influence on the particle assembly at the interface.

The long-range interaction between the substrate and particles may also affect the characterization of the depletion region boundary at different particle densities. A particle on the interface close to the contact line will experience a strong repulsion from the patterned substrate and move towards the droplet apex; this force decays as the distance to the contact line increases. For a higher interfacial density, particles are pushed closer to the contact line, as their own electrostatic repulsion keeps them apart. Therefore, particles at the edge of the assembly feel a higher force keeping them within a well-defined boundary. This is generally observed on droplets with > 5000 interfacial particles, as shown in **Figure 2** and **Figure 4a**. Conversely, for a lower interfacial density, the particles can move farther away from the contact line and consequently have more variation in their equilibrium spacing. This corresponds to the behavior in **Figure 4c**, in which the depletion region does not have a well-defined boundary. There is a continuous variation in particle density from the contact line to the apex, rather than a discrete jump.

Analysis of Interparticle Interactions

We quantify the local ordering of particles using the radial distribution function (RDF) denoted as g(r). The RDF represents the number density of particles as a function of distance from an arbitrary reference particle, such that peaks in the RDF correspond to the most frequent separation distances between particles. We compute g(r) by considering particle pairs with a separation distance in a certain cutoff range (30% of the domain size) and bin these values into a histogram. Then, each bin is normalized by its area A_i and the particle density $\rho = n/(L_x L_y)$ by $g(r_i) = \frac{\langle n_i \rangle}{\rho A_i}$ where n is the total number of particles, L_x and L_y are the dimensions of the ROI where $g(r)$ is calculated, and $\langle n_i \rangle$ is an ensemble average of particle numbers in bin i. In our analysis, we only compare the relative position of peaks, as their absolute magnitude is not important.

In **Figure 5d**, g(r) is calculated using the particle centroids for the entire droplet; **Figure 5a-c** shows a subset of particles at the droplet interface for visual clarity. The droplet volumes are sufficiently small such that the variation in height across the droplet can be ignored for the RDF calculation and analysis. Visual inspection of the particle positions shows some hexagonal ordering (highlighted by light blue particles with 6 neighbors) with defects throughout (light green particles with 5 neighbors and dark red particles with 7 neighbors). The RDF confirms these observations with the ratio of the first two peaks closely matching the ratio for an ideal hexagonal lattice ($\sqrt{3} = 1.732$). The latter peaks are not as well-defined for the triangular droplet due to a significant number of defects present in the structure.

We contend that the hexagonal ordering arises from the confinement of particles caused by the same effect responsible for the depletion region, coupled with electrostatic repulsion between individual particles. It has been well documented that particles can experience attractive forces at

a fluid interface,[5,6,40,41] although the origin of the force is still under debate. However, attractive forces are difficult to investigate at high particle densities when confinement from the substrate dominates the assembly. We conducted additional experiments with a lower interfacial particle density to probe attractive forces between particles, as shown in Video S3. The formation and breakup of linear aggregates clearly indicate the presence of attraction between particles. Interestingly, the dynamical change of the assembly structure implies a time dependence of the attraction. More observations are required to determine if the observed phenomena are caused by slow contact line relaxation[42] that leads to anisotropic capillary interactions, induced in-plane electric dipoles,[43] or other effects. A non-homogenous distribution of charges on the air side of the polystyrene particles would cause an in-plane electric dipole to form. However, it is unknown whether the complex dynamics of particle attachment at the interface could result in an asymmetric charge distribution.

To investigate the location of charges on the interfacial particles, we conducted an experiment with 5 mM NaCl added to the target water droplet as shown in **Figure 6**. The water conductivity was increased by five orders of magnitude, from 0.055 to 705 μS/cm. In this experiment, we observed no change in the particle assembly dynamics. The size of the depletion region and local ordering of particles were similar, and the equilibrium distance on the saltwater droplet was 13.9 μm compared to 17.1 μm on the DI water droplet, a difference of only 3 μm. The higher concentration of ions in the water phase leads to a shorter Debye screening length and a correspondingly weaker repulsive dipolar interaction.[6,44] It appears that the addition of salt screens some of the repulsion between particles, but charges on the air side imparted during electrospray can still dominate their interaction. Furthermore, differences in the RDF could also be attributed to a higher total number of particles delivered to the saltwater droplet, leading to

more confinement and a shorter equilibrium distance. The initial droplet volume was the same for both experiments, but the saltwater droplet evaporated approximately 30% faster. This can be attributed to the difference in ambient relative humidity, which was 10 ± 5% for the salt experiment and 50 ± 5% for the initial experiment. This result indicates that the dielectric particles remain highly charged on the air side and is consistent with our theory of depletion region formation.

Additional experiments with a non-volatile fluid, ETPTA (trimethylolpropane ethoxylate triacrylate) are provided in the SI. The electrospray parameters were similar between the water and the ETPTA experiments. A schematic of particles on different target droplets is shown in **Figure 7**. The experimental observations shown in **Figure 4** are illustrated and explained in **Figure 7a, b**. The depletion region only forms on water droplets with a surface energy pattern, as charges are not able to dissipate through the photoresist before the end of evaporation. The charges on the air side of the particles are primarily responsible for both the repulsion from the substrate and the interparticle repulsion leading to a uniform separation distance. Also, charges from the electrospray deposited to the water-air interface (in the space between particles) may be neutralized or screened via dissolved ions. However, ETPTA does not contain screening ions, so electric charges are distributed across the entire particle surface and ETPTA interface as shown in **Figure 7c**. This leads to an amorphous structure, where particles have negligible electrostatic repulsion and do not maintain a uniform separation distance over time. Furthermore, the contact angle of polystyrene particles at the ETPTA-air interface (measured in the liquid phase) is less than 90° so the maximum net repulsion between particles is also reduced, as less charge is exposed to the air side.[45]

Conclusion

In this study, we have used electrospray printing for the delivery of microparticles to a geometrically controlled liquid interface. Non-functionalized fluorescent polystyrene particles were selected for their optical and dielectric properties. The number of particles delivered was determined by the electrospray parameters, including spray time, solution concentration, and flow rate. We created patterned substrates with a 50 μm thick SU-8 photoresist layer, which retained a net electric charge after the spray was stopped. The colloidal assembly at the target droplet interface was dominated by electrostatic repulsions between the particles and the surrounding dielectric substrate. For three characteristic shapes (circle, triangle, dumbbell), a common phenomenon was the formation of a depletion region near the contact line, as particles preferentially assembled at the center of the droplet. The depletion region was maintained over the course of evaporation, up to 25 min for the highest initial droplet volume of 2.5 μl. For unpatterned, FTO coated substrates, the targeted droplets did not exhibit a depletion region as deposited charge on the surrounding area was able to dissipate immediately. We found that the sprayed particles must remain highly charged on the air side, by observing minimal changes in the particle assembly on a droplet with added salt. Additionally, we targeted droplets of a non-volatile organic solvent, ETPTA. Particles did not assemble into hierarchical structures on ETPTA owing to its different dielectric properties compared to water.

Further experiments probing the attractive potential between particles may be useful for determining the expected colloidal assembly in the absence of substrate repulsion. The observed "snapping" and "un-snapping" phenomenon in the supplemental video (Video S3) indicates a system far from equilibrium. The cause for this fascinating assembly may lie in the particles' contact line undulation and relaxation over time. Based on our data and method for particle

delivery, reconfiguration of charges at the interface may also be responsible for the sudden rearrangement of particles. Variations in the electrospray parameters and operating conditions will almost certainly affect the uniformity of charge on the particle surface.

Figures

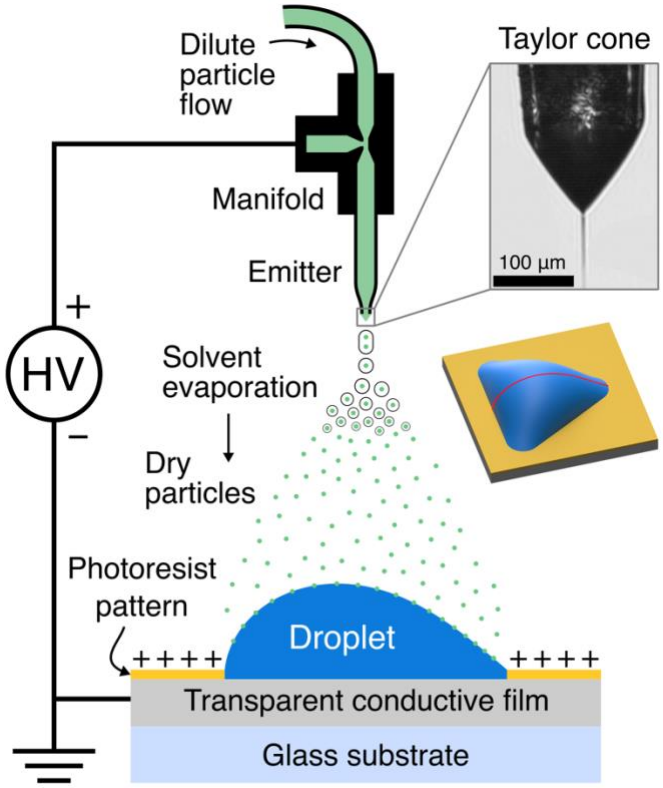

Figure 1. Cross-section of interfacial particle delivery by electrospray printing. The asymmetric 2D droplet geometry corresponds to the triangular 3D droplet mid-plane, indicated by the red line. To generate the electrospray, a dilute suspension of microparticles is pumped through a manifold and glass emitter. The high voltage applied between the emitter and conductive coating creates a strong electric field, which directs charged particles towards the target droplet. The volatile solvent encapsulating the particles completely evaporates before the particles reach the droplet surface. The droplet shape is fixed by pinning the contact line to SU-8 photoresist patterns. Charge accumulates on the electrically insulative photoresist and repels incoming particles, which directs more particles to the fluid interface.

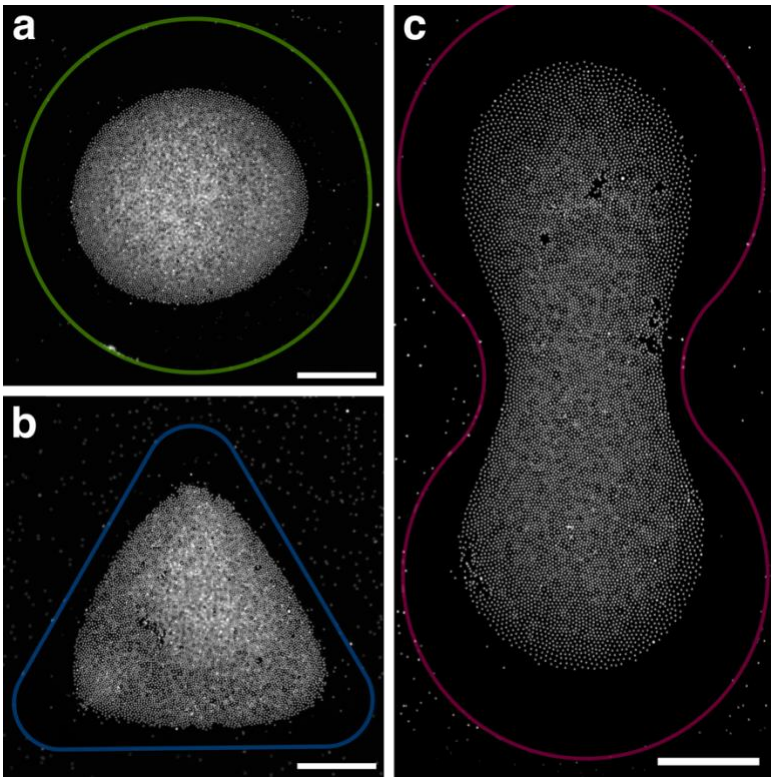

Figure 2. Fluorescent particles on the interface of water droplets (top view). The pinned contact line geometry is highlighted with a colored line. The spherical cap droplet (a) exhibits a uniform depletion region around the majority of the contact line. The depletion region on the triangle (b) and dumbbell (c) droplets varies with position. The volume of each droplet (a, b, c) was 0.2, 0.30, and 0.25 µl, respectively. Scale bars are 500 µm for all images.

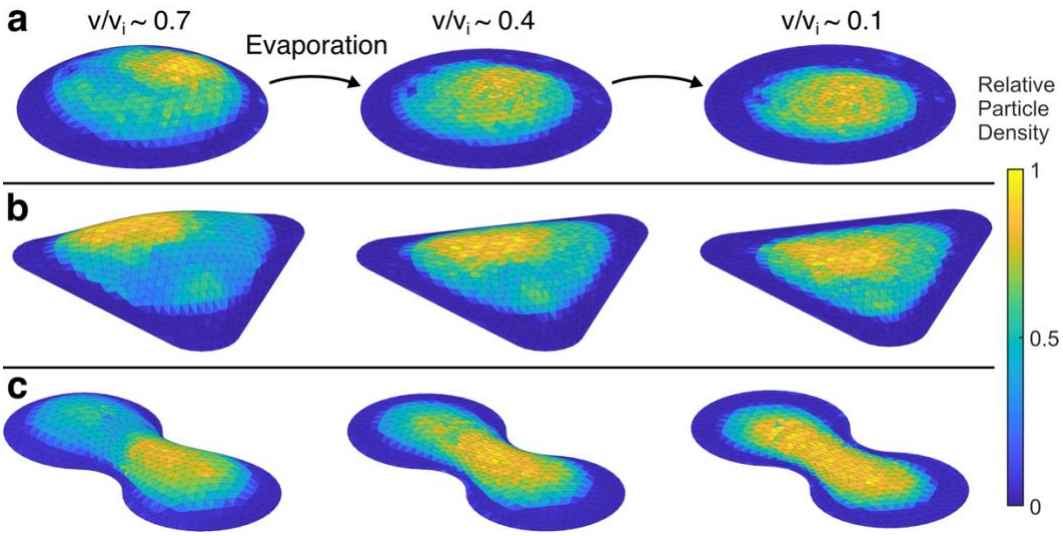

Figure 3. Relative particle density mapped to 3 different water droplet shapes: circle (a), triangle (b), and dumbbell (c) at descending volumes during evaporation. The amount of liquid remaining is indicated by the dimensionless ratio v/v_i where v_i is the initial droplet volume and v is the instantaneous volume. When $v/v_i = 0.7$, the highest density region is not centered on the droplet interface. Over time the particle distribution homogenizes radially, and the density decreases gradually from the center until a sharp decline at the depletion region where the density is zero. The shape of the depletion region is consistent over time, until the late stage of evaporation (not shown).

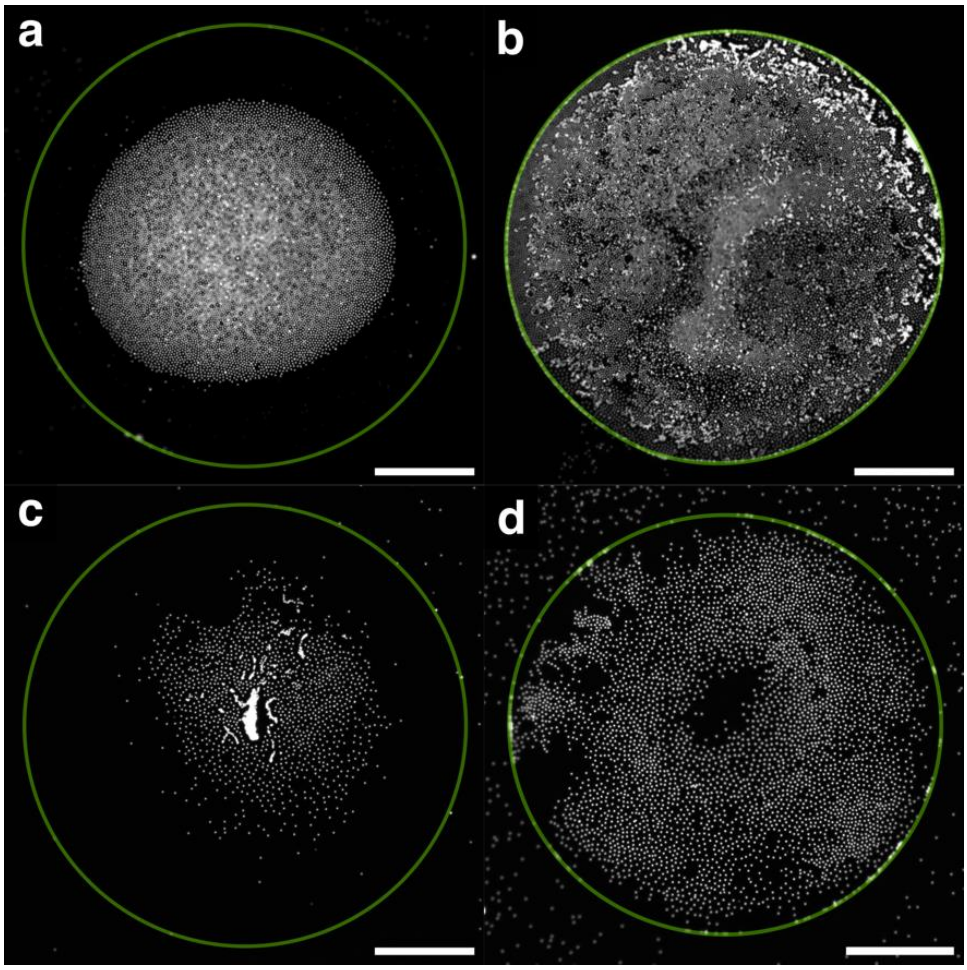

Figure 4. Targeting Droplets without Surface Energy Patterning

Particles on axisymmetric water droplets, with the circular contact line highlighted in color. The volume of each droplet was less than 0.40 µl; approximately 25% of the initial volume was remaining. The contact line was defined by two methods: an SU-8 pattern for (a) and (c), and by surface chemistry alone for (b) and (d). The presence of an electrically insulating SU-8 pattern causes a depletion region to form due to the accumulation of electric charge; without this dielectric barrier particles are able to move freely near the contact line. The number of particles delivered to (a) and (b) was > 11500, compared to < 5000 for (c) and (d). The depletion region forms on droplets with SU-8 patterns regardless of particle density, and the boundary becomes more well defined with increasing particle delivery.

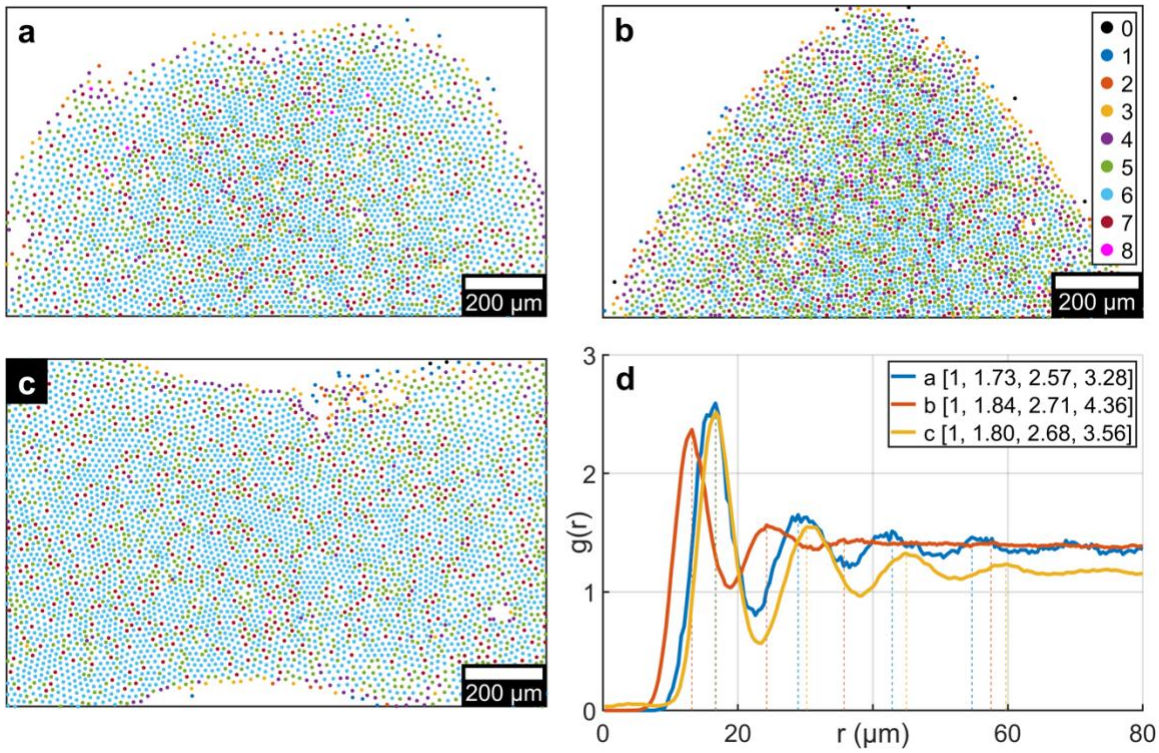

Figure 5. Local Particle Structure

Particle positions on a circular (a), triangular (b), and dumbbell (c) shaped water droplet; the volumes for each droplet were 0.2, 0.24, and 0.3 µl, respectively. The particle color corresponds to the number of nearest neighbors. The radial distribution function (d) shows distinct peaks for all droplet shapes, and the values in the legend correspond to the ratio of the peak positions. The peak ratios for an ideal hexagonal lattice are [1, 1.73, 2, 2.65, 3].

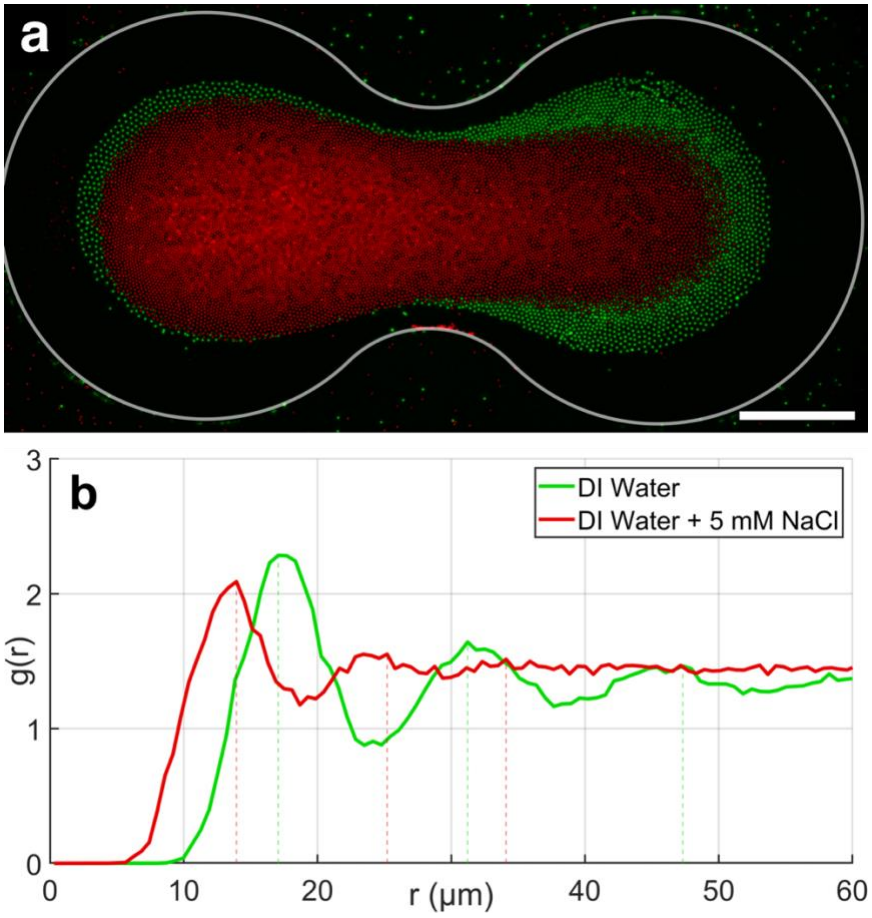

Figure 6. Particles on a dumbbell shaped DI water droplet (a) without added salt (green) and with 5 mM NaCl added (red). The images were taken close to the end of evaporation; the volume of each droplet was 0.17 and 0.1 µl, respectively. The number of particles delivered to droplet without added salt was ≈ 9000, compared to ≈ 11000 for the droplet with salt. The radial distribution function (b) indicates a larger primary equilibrium distance of 17.1 µm for the salt-free water droplet compared to 13.9 µm for the saltwater droplet.

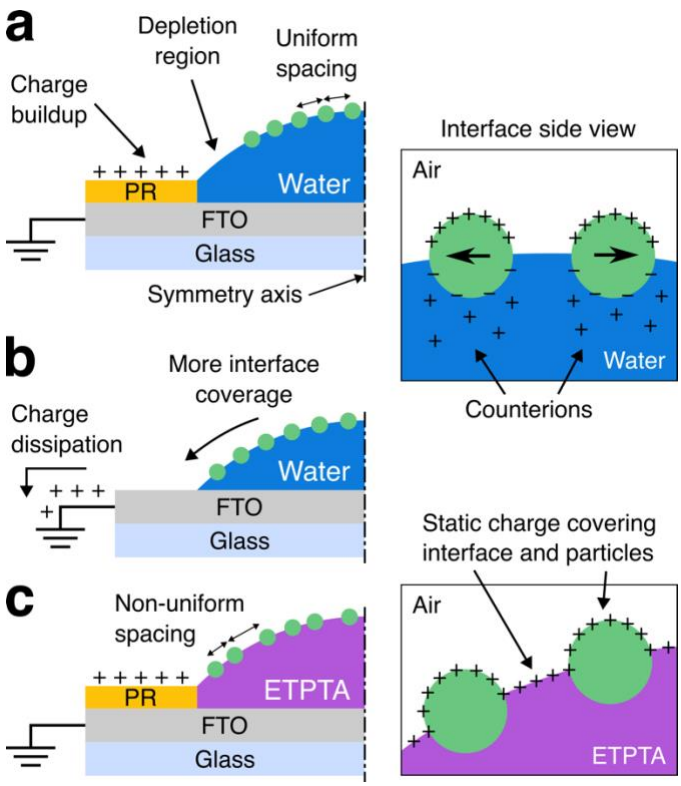

Figure 7. Representation of a spherically symmetric target droplet (a) with charged particles at a water-air interface. Electrostatic repulsion from charges on the patterned photoresist leads to the depletion region formation. The particles remain charged on the air side from the electrospray as shown in the magnified side view, driving interparticle repulsions and a consistent equilibrium distance over time. A droplet without the pattern (b) does not exhibit a depletion region, as charge on the conductive FTO substrate is able to dissipate much faster than the time scale for evaporation. For a non-volatile organic solvent (c), the depletion region does not form, and the spacing between particles varies with time and position. Charges from the electrospray at the ETPTA-air interface are not able to neutralize through the liquid phase, so there is negligible interparticle or particle-substrate repulsion.

Author Information

Corresponding Authors

*Paul R. Chiarot, pchiarot@binghamton.edu

[+]Xin Yong, xyong@binghamton.edu

Supporting Information

- Additional experiments on substrates with a thinner photoresist pattern, and a non-volatile target droplet fluid (.pdf)
- *In situ* observation of electrospray deposition onto an air-water interface (.mp4)
- Particle assembly on dumbbell droplet after electrospray is complete (.mp4)
- Formation and breakup of networked structures on unpatterned water droplet (.mp4)

Acknowledgements

This research was supported by the National Science Foundation (Award 1939362).

References

(1) Pieranski, P. Two-Dimensional Interfacial Colloidal Crystals. *Phys Rev Lett* **1980**, *45* (7), 569–572. https://doi.org/10.1103/PhysRevLett.45.569.

(2) Cavallaro, M.; Botto, L.; Lewandowski, E. P.; Wang, M.; Stebe, K. J. Curvature-Driven Capillary Migration and Assembly of Rod-like Particles. *Proceedings of the National Academy of Sciences* **2011**, *108* (52), 20923–20928. https://doi.org/10.1073/pnas.1116344108.

(3) Kumar, A.; Park, B. J.; Tu, F.; Lee, D. Amphiphilic Janus Particles at Fluid Interfaces. *Soft Matter* **2013**, *9* (29), 6604–6617. https://doi.org/10.1039/C3SM50239B.

(4) Madivala, B.; Fransaer, J.; Vermant, J. Self-Assembly and Rheology of Ellipsoidal Particles at Interfaces. *Langmuir* **2009**, *25* (5), 2718–2728. https://doi.org/10.1021/la803554u.

(5) Stamou, D.; Duschl, C.; Johannsmann, D. Long-Range Attraction between Colloidal Spheres at the Air-Water Interface: The Consequence of an Irregular Meniscus. *Phys Rev E* **2000**, *62* (4 B), 5263–5272. https://doi.org/10.1103/PhysRevE.62.5263.

(6) Nikolaides, M. G.; Bausch, A. R.; Hsu, M. F.; Dinsmore, A. D.; Brenner, M. P.; Gay, C.; Weitz, D. A. Electric-Field-Induced Capillary Attraction between like-Charged Particles at Liquid Interfaces. *Nature* **2002**, *420* (6913), 299–301. https://doi.org/10.1038/nature01113.

(7) Megens, M.; Aizenberg, J. Like-Charged Particles at Liquid Interfaces. *Nature* **2003**, *424* (6952), 1014. https://doi.org/10.1038/4241014a.

(8) Forth, J.; Kim, P. Y.; Xie, G.; Liu, X.; Helms, B. A.; Russell, T. P. Building Reconfigurable Devices Using Complex Liquid–Fluid Interfaces. *Advanced Materials* **2019**, *31* (18), 1806370. https://doi.org/10.1002/adma.201806370.

(9) Oettel, M.; Dietrich, S. Colloidal Interactions at Fluid Interfaces. *Langmuir* **2008**, *24* (4), 1425–1441. https://doi.org/10.1021/la702794d.

(10) Danov, K. D.; Kralchevsky, P. A. Electric Forces Induced by a Charged Colloid Particle Attached to the Water-Nonpolar Fluid Interface. *J Colloid Interface Sci* **2006**, *298* (1), 213–231. https://doi.org/10.1016/j.jcis.2005.12.037.

(11) Liu, I. B.; Bigazzi, G.; Sharifi-Mood, N.; Yao, L.; Stebe, K. J. Curvature Capillary Repulsion. *Phys Rev Fluids* **2017**, *2* (10), 100501. https://doi.org/10.1103/PhysRevFluids.2.100501.

(12) Würger, A. Curvature-Induced Capillary Interaction of Spherical Particles at a Liquid Interface. *Phys Rev E Stat Nonlin Soft Matter Phys* **2006**, *74* (4), 1–9. https://doi.org/10.1103/PhysRevE.74.041402.

(13) Ershov, D.; Sprakel, J.; Appel, J.; Cohen Stuart, M. A.; van der Gucht, J. Capillarity-Induced Ordering of Spherical Colloids on an Interface with Anisotropic Curvature. *Proceedings of the National Academy of Sciences* **2013**, *110* (23), 9220–9224. https://doi.org/10.1073/pnas.1222196110.

(14) Sefiane, K. Patterns from Drying Drops. *Adv Colloid Interface Sci* **2014**, *206*, 372–381. https://doi.org/10.1016/j.cis.2013.05.002.

(15) Deegan, R. D.; Bakajin, O.; Dupont, T. F.; Huber, G.; Nagel, S. R.; Witten, T. A. Capillary Flow as the Cause of Ring Stains from Dried Liquid Drops. *Nature* **1997**, *389* (6653), 827–829. https://doi.org/10.1038/39827.

(16) Hu, H.; G. Larson, R. Analysis of the Effects of Marangoni Stresses on the Microflow in an Evaporating Sessile Droplet. *Langmuir* **2005**, *21* (9), 3972–3980. https://doi.org/10.1021/la0475270.

(17) Marin, A.; Liepelt, R.; Rossi, M.; Kä, C. J. Surfactant-Driven Flow Transitions in Evaporating Droplets. *Royal Society of Chemistry* **2016**, *12*, 1593–1600. https://doi.org/10.1039/c5sm02354h.

(18) Ghafouri, A.; Zhao, M.; Singler, T. J.; Yong, X.; Chiarot, P. R. Interfacial Targeting of Sessile Droplets Using Electrospray. *Langmuir* **2018**, *34* (25), 7445–7454. https://doi.org/10.1021/acs.langmuir.8b01308.

(19) Al-Milaji, K. N.; Secondo, R. R.; Ng, T. N.; Kinsey, N.; Zhao, H. Interfacial Self-Assembly of Colloidal Nanoparticles in Dual-Droplet Inkjet Printing. *Adv Mater Interfaces* **2018**, *5* (10), 1–11. https://doi.org/10.1002/admi.201701561.

(20) Shin, D.; Huang, T.; Neibloom, D.; Bevan, M. A.; Frechette, J. Multifunctional Liquid Marble Compound Lenses. *ACS Appl Mater Interfaces* **2019**, *11* (37), 34478–34486. https://doi.org/10.1021/acsami.9b12738.

(21) Cai, Z.; Li, Z.; Ravaine, S.; He, M.; Song, Y.; Yin, Y.; Zheng, H.; Teng, J.; Zhang, A. From Colloidal Particles to Photonic Crystals: Advances in Self-Assembly and Their Emerging Applications. *Chem Soc Rev* **2021**, *50* (10), 5898–5951. https://doi.org/10.1039/D0CS00706D.

(22) Fujii, S.; Kappl, M.; Butt, H. J.; Sugimoto, T.; Nakamura, Y. Soft Janus Colloidal Crystal Film. *Angewandte Chemie - International Edition* **2012**, *51* (39), 9809–9813. https://doi.org/10.1002/anie.201204358.

(23) Zhang, J.-T.; Wang, L.; Luo, J.; Tikhonov, A.; Kornienko, N.; Asher, S. A. 2-D Array Photonic Crystal Sensing Motif. *J Am Chem Soc* **2011**, *133* (24), 9152–9155. https://doi.org/10.1021/ja201015c.

(24) Zhang, J.-T.; Smith, N.; Asher, S. A. Two-Dimensional Photonic Crystal Surfactant Detection. *Anal Chem* **2012**, *84* (15), 6416–6420. https://doi.org/10.1021/ac300174m.

(25) Li, C.; Lotsch, B. v. Stimuli-Responsive 2D Polyelectrolyte Photonic Crystals for Optically Encoded PH Sensing. *Chemical Communications* **2012**, *48* (49), 6169–6171. https://doi.org/10.1039/C2CC31916K.

(26) Ye, X.; Li, Y.; Dong, J.; Xiao, J.; Ma, Y.; Qi, L. Facile Synthesis of ZnS Nanobowl Arrays and Their Applications as 2D Photonic Crystal Sensors. *J Mater Chem C Mater* **2013**, *1* (38), 6112–6119. https://doi.org/10.1039/C3TC30118D.

(27) Kiyomi, Y.; Shiraiwa, N.; Nakazawa, T.; Fukawa, A.; Oshio, K.; Takase, K.; Ito, T.; Shingubara, S.; Shimizu, T. Fabrication and UV Photoresponse of Ordered ZnO Nanonets Using Monolayer Colloidal Crystal Template. *Micro and Nano Engineering* **2022**, *16*, 100160. https://doi.org/10.1016/J.MNE.2022.100160.

(28) Noguera-Marín, D.; Moraila-Martínez, C. L.; Cabrerizo-Vílchez, M. A.; Rodríguez-Valverde, M. A. In-Plane Particle Counting at Contact Lines of Evaporating Colloidal Drops: Effect of the Particle Electric Charge. *Soft Matter* **2015**, *11* (5), 987–993. https://doi.org/10.1039/C4SM02693D.

(29) Noguera-Marín, D.; Moraila-Martínez, C. L.; Cabrerizo-Vílchez, M. A.; Rodríguez-Valverde, M. A. Particle Segregation at Contact Lines of Evaporating Colloidal Drops: Influence of the Substrate Wettability and Particle Charge–Mass Ratio. *Langmuir* **2015**, *31* (24), 6632–6638. https://doi.org/10.1021/acs.langmuir.5b01062.

(30) Kingsley, B. J.; Pawliczak, E. E.; Hurley, T. R.; Chiarot, P. R. Electrospray Printing of Polyimide Films Using Passive Material Focusing. *ACS Appl Polym Mater* **2021**, *3* (12), 6274–6284. https://doi.org/10.1021/acsapm.1c01073.

(31) Zhu, Y.; Chiarot, P. R. Directed Assembly of Nanomaterials Using Electrospray Deposition and Substrate-Level Patterning. *Powder Technol* **2020**, *364*, 845–850. https://doi.org/10.1016/j.powtec.2020.01.066.

(32) Zhu, Y.; Chiarot, P. R. Surface Charge Accumulation and Decay in Electrospray Printing. *J Phys D Appl Phys* **2021**, *54* (7), 075301. https://doi.org/10.1088/1361-6463/abc449.

(33) Khalilur Rahman, Md.; Huy Phung, T.; Oh, S.; Hyun Kim, S.; Nga Ng, T.; Kwon, K.-S. High-Efficiency Electrospray Deposition Method for Nonconductive Substrates: Applications of Superhydrophobic Coatings. *ACS Appl Mater Interfaces* **2021**, *13* (15), 18227–18236. https://doi.org/10.1021/acsami.0c22867.

(34) Sikanen, T.; Tuomikoski, S.; Ketola, R. A.; Kostiainen, R.; Franssila, S.; Kotiaho, T. Characterization of SU-8 for Electrokinetic Microfluidic Applications. *Lab Chip* **2005**, *5* (8), 888–896. https://doi.org/10.1039/B503016A.

(35) Birdi, K. S.; Vu, D. T.; Winter, A. A Study of the Evaporation Rates of Small Water Drops Placed on a Solid Surface. *J Phys Chem* **1989**, *93* (9), 3702–3703. https://doi.org/10.1021/j100346a065.

(36) Sáenz, P. J.; Wray, A. W.; Che, Z.; Matar, O. K.; Valluri, P.; Kim, J.; Sefiane, K. Dynamics and Universal Scaling Law in Geometrically-Controlled Sessile Drop Evaporation. *Nat Commun* **2017**, *8*, 1–9. https://doi.org/10.1038/ncomms14783.

(37) Larson, R. G. In Retrospect: Twenty Years of Drying Droplets. *Nature*. 2017, pp 466–467. https://doi.org/10.1038/550466a.

(38) Hu, H.; Larson, R. G. Analysis of the Microfluid Flow in an Evaporating Sessile Droplet. *Langmuir* **2005**, *21* (9), 3963–3971. https://doi.org/10.1021/la047528s.

(39) Ristenpart, W. D.; Kim, P. G.; Domingues, C.; Wan, J.; Stone, H. A. Influence of Substrate Conductivity on Circulation Reversal in Evaporating Drops. *Phys Rev Lett* **2007**, *99* (23), 234502. https://doi.org/10.1103/PhysRevLett.99.234502.

(40) Würger, A. Capillary Attraction of Charged Particles at a Curved Liquid Interface. *Europhys Lett* **2006**, *75* (6), 978–984. https://doi.org/10.1209/epl/i2006-10209-3.

(41) Liu, I. B.; Sharifi-Mood, N.; Stebe, K. J. Capillary Assembly of Colloids: Interactions on Planar and Curved Interfaces. *Annu Rev Condens Matter Phys* **2018**, *9* (1), 283–305. https://doi.org/10.1146/annurev-conmatphys-031016-025514.

(42) Kaz, D. M.; McGorty, R.; Mani, M.; Brenner, M. P.; Manoharan, V. N. Physical Ageing of the Contact Line on Colloidal Particles at Liquid Interfaces. *Nat Mater* **2012**, *11* (2), 138–142. https://doi.org/10.1038/nmat3190.

(43) Chen, W.; Tan, S.; Huang, Z.; Ng, T. K.; Ford, W. T.; Tong, P. Measured Long-Ranged Attractive Interaction between Charged Polystyrene Latex Spheres at a Water-Air Interface. *Phys Rev E Stat Nonlin Soft Matter Phys* **2006**, *74* (2), 1–14. https://doi.org/10.1103/PhysRevE.74.021406.

(44) Park, B. J.; Pantina, J. P.; Furst, E. M.; Oettel, M.; Reynaert, S.; Vermant, J. Direct Measurements of the Effects of Salt and Surfactant on Interaction Forces between Colloidal Particles at Water−Oil Interfaces. *Langmuir* **2008**, *24* (5), 1686–1694. https://doi.org/10.1021/la7008804.

(45) Danov, K. D.; Kralchevsky, P. A. Forces Acting on Dielectric Colloidal Spheres at a Water/Nonpolar Fluid Interface in an External Electric Field. 2. Charged Particles. *J Colloid Interface Sci* **2013**, *405*, 269–277. https://doi.org/10.1016/J.JCIS.2013.05.015.

Table of Contents Graphic